01 Jun 1990

Coupled-Channel Optical Calculation of Electron-Hydrogen Scattering: The Distorted-Wave Optical Potential

Igor Bray

Don H. Madison
Missouri University of Science and Technology, madison@mst.edu

Ian E. McCarthy

Recommended Citation

I. Bray et al., "Coupled-Channel Optical Calculation of Electron-Hydrogen Scattering: The Distorted-Wave Optical Potential," *Physical Review A - Atomic, Molecular, and Optical Physics*, vol. 41, no. 11, pp. 5916-5928, American Physical Society (APS), Jun 1990.
The definitive version is available at https://doi.org/10.1103/PhysRevA.41.5916

Coupled-channel optical calculation of electron-hydrogen scattering: The distorted-wave optical potential

I. Bray
Institute for Atomic Studies, The Flinders University of South Australia, Bedford Park, South Australia 5042, Australia

D. H. Madison
Department of Physics, University of Missouri–Rolla, Rolla, Missouri 65401

I. E. McCarthy
Institute for Atomic Studies, The Flinders University of South Australia, Bedford Park, South Australia 5042, Australia
(Received 17 January 1990)

The coupled-channel optical method solves a set of coupled momentum-space integral equations for a finite set of reaction channels. The remaining channels, including the target continuum, are described by the polarization potential operator, which formally depends on the full three-body state vectors for these channels. The distorted-wave optical potential makes the distorted-wave Born approximation for these state vectors, using exact target states. No other approximation is made. Calculations and comparison with experiment are reported for total ionization cross sections and asymmetries, total excitation cross sections, entrance-channel phenomena, and the coupled $1s, 2s, 2p$ channels, at a range of energies.

I. INTRODUCTION

This is the third in a series of papers on the momentum-space coupled-channel optical (CCO) method for electron-atom scattering. The first[1] dealt with the coupled equations for a one-electron target. The second[2] treated many-electron targets and the distorted-wave representation, which enables charged targets to be included and reduces the computational labor.

The CCO method is a fully microscopic, nonperturbative method for calculating electron-atom scattering, in which channels in a finite set (P space) are explicitly coupled and the remaining channels (Q space), including the target continuum, are included in a complex, nonlocal polarization potential. Up to now it has been necessary to make analytic approximations[3] to the excitation matrix elements in the polarization potential and to make further approximations[3,4] for computational feasibility. Here we use exact target eigenstates for hydrogen in both the bound and continuum cases. The only approximation is that the three-body wave functions for excitations into Q space are approximated by the product of the corresponding target eigenstate and an elastic scattering function (distorted wave) calculated in the appropriate potential. A preliminary calculation[5] of elastic scattering in this approximation made the additional approximation of omitting exchange terms from the polarization potential. Here exchange is fully treated.

Other nonperturbative calculations of electron-hydrogen scattering at intermediate energies include the intermediate-energy R-matrix method[6,7] (IERM), in which the numerical solution of the three-body Schrödinger equation in a finite, spherical region is matched to two-body external boundary conditions and the resulting T-matrix elements are averaged over pseudoresonances. This is also a fully microscopic method. The unitarized eikonal-Born series[8] (UEBS) is an essentially nonperturbative semiclassical method. The calculation that most resembles the present one is the pseudostate method[9,10] (PS), in which Q space is represented by a set of orthogonal and normalized square-integrable pseudostate functions with low values of orbital angular momentum. These functions play the same part in the computation as discrete target states, so that the resulting pseudoproblem can be solved to numerical convergence. The parameters of the pseudoproblem are chosen in various ways such as diagonalizing the atomic Hamiltonian or requiring the pseudostate basis set to reproduce some known result such as the atomic polarizability or the second Born amplitude.

A perturbative method that is directly related to the present calculation is the exact second-order distorted-wave approximation of Madison, Hughes, and McGinness.[11] In that work the three-body wave functions occurring in the sum over intermediate states in the second-order T matrix are approximated as a product of target wave functions and a distorted wave. The important advancement represented by that work, and used here, is the exact integration over the target continuum. With the addition of exchange terms[12] the matrix elements of that approximation are the driving terms of the integral equations of the CCO method in the distorted-wave representation.

The *a priori* justification of the distorted-wave optical potential depends on the validity of the distorted-wave Born approximation (DWBA) for describing experimental cross sections. It has had success in describing discrete excitations[13] and recent detailed comparisons

with $(e,2e)$ data[14] have shown that it gives a good account of the large differential cross sections that are particularly relevant to the kinematic integration space of the polarization potential. Nevertheless, like all present scattering methods, it does not satisfy the three-body boundary conditions for charged particles.[15] Formally a three-body ansatz such as that of Brauner, Briggs, and Klar,[15] which is very successful in describing $(e,2e)$ data, can be included in the distorted-wave optical potential. The computation is very difficult.

Section II gives a full formal derivation of the CCO method. Section III describes the distorted-wave (DW) optical potential and Sec. IV discusses its numerical implementation. In Sec. V we form some *a priori* ideas of the validity of the DW optical potential at different energies by calculating total ionization cross sections and asymmetries and total excitation cross sections in the weak-coupling approximation and comparing them with experiment. Section VI discusses entrance-channel phenomena in which P space consists only of the $1s$ channel. Section VII discusses scattering in the $1s,2s,2p$ P space.

II. FORMAL DERIVATION OF THE CCO METHOD

The total Hamiltonian for the electron-hydrogen problem is

$$H=K+V \ , \tag{1}$$

where

$$K=K_1+K_2+v_2 \ , \tag{2}$$

$$V=v_1+v_3 \ . \tag{3}$$

The kinetic energies of electrons 1 and 2 are K_1 and K_2. The corresponding electron-nucleus potentials are v_1 and v_2. The electron-electron potential is v_3.

Channel states Φ_μ are defined as

$$(E_\mu-K)|\Phi_\mu\rangle=0 \ , \tag{4}$$

$$|\Phi_\mu\rangle=|j\mathbf{k}_\mu\rangle \ , \tag{5}$$

where j denotes a target eigenstate

$$(\varepsilon_j-K_2-v_2)|j\rangle=0 \tag{6}$$

and $\mathbf{k}_\mu$ is the momentum of the projectile electron. In the case of ionized target states, j and μ constitute a discrete notation for the continuum which is formally convenient but will be replaced when necessary by explicit continuum notation.

The Schrödinger equation for the whole problem is

$$(E^{(\pm)}-K)|\Psi_0^{(\pm)}(\mathbf{k}_0)\rangle=V|\Psi_0^{(\pm)}(\mathbf{k}_0)\rangle \ , \tag{7}$$

where $\Psi_0^{(\pm)}(\mathbf{k}_0)$ describes the scattering of a projectile of momentum $\mathbf{k}_0$ incident on the ground state of the target. Superscripts $(\pm)$ indicate ingoing or outgoing spherical-wave boundary conditions, respectively.

Antisymmetry[16] is introduced into the formalism by replacing V in (7) with V_S, defined by

$$\langle i|V_S|j\rangle=\langle i|v_3[1+(-1)^S P_r]|j\rangle + \delta_{ij}\left[v_1+\sum_k (1-S\delta_{ij})(\varepsilon_i+\varepsilon_k-E)\right] \ , \tag{8}$$

where S is the total electron spin and P_r is the space-exchange operator. This form ensures uniqueness and stability of off-shell solutions of the integral equation corresponding to (7) and enables the electron-hydrogen problem to be treated by the formalism of multichannel two-body scattering theory. For nonrelativistic scattering S is a good quantum number. We will drop it from the formalism until we need it.

The space of target states is divided into two by the projection operators P and Q, defined by

$$P=\sum_{j\in P}|j\rangle\langle j| \ , \tag{9}$$

$$P+Q=1 \ . \tag{10}$$

Using these definitions we obtain the P-projected form of the Schrödinger equation (7):

$$P(E^{(+)}-K-V)P|\Psi_0^{(+)}\rangle=PVQ|\Psi_0^{(+)}\rangle \ . \tag{11}$$

Substituting $Q|\Psi_0^{(+)}\rangle$ from the corresponding Q-projected equation we obtain

$$P(E^{(+)}-K-V-V^{(Q)})P|\Psi_0^{(+)}\rangle=0 \ , \tag{12}$$

where the polarization potential $V^{(Q)}$ is defined by

$$PV^{(Q)}P|\Psi_0^{(+)}\rangle=P\left[VQ\frac{1}{Q(E^{(+)}-K-V)Q}QV\right]P|\Psi_0^{(+)}\rangle \ . \tag{13}$$

The integral equation corresponding to (12) is

$$|\Psi_0^{(+)}\rangle=|\Psi_0\rangle+\frac{1}{P(E^{(+)}-K)P}P(V+V^{(Q)})P|\Psi_0^{(+)}\rangle \ . \tag{14}$$

We now define the P-projected T-matrix element and rearrange it using the identity obtained from (11) and (12):

$$PVQ|\Psi_0^{(+)}\rangle=PV^{(Q)}P|\Psi_0^{(+)}\rangle \ . \tag{15}$$

The P-projected T-matrix element is

$$\langle\Phi_\mu|PT|\Phi_0\rangle=\langle\Phi_\mu|PV|\Psi_0^{(+)}\rangle \tag{16}$$

$$=\langle\Phi_\mu|PV(P+Q)|\Psi_0^{(+)}\rangle$$

$$=\langle\Phi_\mu|P(V+V^{(Q)})P|\Psi_0^{(+)}\rangle \ . \tag{17}$$

We obtain the coupled Lippman-Schwinger equations for the P-projected T-matrix elements by substituting the form (14) for $|\Psi_0^{(+)}\rangle$ in (17) and using definition (16):

$$\langle\Phi_\mu|PT|\Phi_0\rangle=\langle\Phi_\mu|P(V+V^{(Q)})|\Phi_0\rangle + \sum_\nu\langle\Phi_\mu|P(V+V^{(Q)})P|\Phi_\nu\rangle \times\frac{1}{E^{(+)}-E_\nu}\langle\Phi_\nu|PT|\Phi_0\rangle \ . \tag{18}$$

We now make the continuum notation explicit in (18) by using definition (5) of $|\Phi_\mu\rangle$ and reintroduce the spin subscript S:

$$\langle \mathbf{k}i|T_S|0\mathbf{k}_0\rangle = \langle \mathbf{k}i|V_S+V_S^{(Q)}|0\mathbf{k}_0\rangle + \sum_{j\in P}\int d^3q\,\langle \mathbf{k}i|V_S+V_S^{(Q)}|j\mathbf{q}\rangle \times \frac{1}{E^{(+)}-\varepsilon_j-\frac{1}{2}q^2} \times \langle \mathbf{q}j|T_S|0\mathbf{k}_0\rangle, \quad i\in P\ . \tag{19}$$

This is the set of coupled Lippman-Schwinger equations that is solved[1] for the P-space T-matrix elements.

III. THE DISTORTED-WAVE POLARIZATION POTENTIAL

The matrix elements of the formal polarization potential (13) are written in terms of explicit excitation amplitudes for states in Q space by inserting the complete set $\Psi_\mu^{(-)}$ of exact eigenstates of the three-body problem:

$$\langle \mathbf{q}'i|V_S^{(Q)}|j\mathbf{q}\rangle = \sum_{\nu\in Q}\langle \mathbf{q}'i|V_S|\Psi_\nu^{(-)}\rangle \times \frac{1}{E^{(+)}-E_\nu^{(-)}}\langle \Psi_\nu^{(-)}|V_S|j\mathbf{q}\rangle\ . \tag{20}$$

Together with the P-projected integral equations (18), this constitutes a rearrangement of the electron-hydrogen problem in which the target continuum can be made formally explicit. We have not solved the problem of course, since the $\Psi_\nu^{(-)}$ have not been found.

The CCO method removes the difficulties of solving the problem to Q space. The three-body wave functions of Q space are of three kinds, which we approximate as follows, writing the target eigenstate first.

(1) Two electrons in the continuum:

$$|\Psi_\nu^{(-)}\rangle = |\chi^{(-)}(\mathbf{k})\rangle|\chi_c^{(-)}(\mathbf{k}')\rangle\ , \tag{21a}$$

(2) One electron in a bound state p:

$$|\Psi_\nu^{(-)}\rangle = |p\rangle\chi_p^{(-)}(\mathbf{k}')\rangle\ , \tag{21b}$$

(3) Three-body bound state: omitted.

We do not believe the single three-body bound state will affect the calculation.

Using approximation (21) for the three-body states we write the distorted-wave polarization potential as the sum of two terms, one each for discrete and continuum target states:

$$\langle \mathbf{q}'i|V_S^{(Q)}|j\mathbf{q}\rangle = \sum_{p\in Q}\tfrac{1}{2}\langle \mathbf{q}'i|V_S|p\rangle\left[\int d^3k'|\chi_p^{(-)}(\mathbf{k}')\rangle\frac{1}{E^{(+)}-\varepsilon_p-\frac{1}{2}k'^2}\langle\chi_p^{(-)}(\mathbf{k}')|\right]\langle p|V_S|j\mathbf{q}\rangle + \int d^3k\tfrac{1}{4}\langle \mathbf{q}'i|V_S|\chi^{(-)}(\mathbf{k})\rangle\left[\int d^3k'|\chi_c^{(-)}(\mathbf{k}')\rangle\frac{1}{E^{(+)}-\frac{1}{2}(k'^2+k^2)}\langle\chi_c^{(-)}(\mathbf{k}')|\right]\langle\chi^{(-)}(\mathbf{k})|V_S|j\mathbf{q}\rangle\ . \tag{22}$$

The factor $\frac{1}{2}$ in the discrete sum comes from the normalization of the 2×2 determinants constituting the antisymmetrized wave functions. The extra factor $\frac{1}{2}$ in the continuum integral ensures that the states are not double counted in the double integration over the momenta of indistinguishable electrons.

The distorted waves $\chi_p^{(-)}(\mathbf{k}'),\chi_c^{(-)}(\mathbf{k}')$ represent electrons scattered elastically from the potential U, which is different in different cases.

(1) Two electrons in the continuum:

$$U = v_1\ , \tag{23a}$$

(2) One electron in a bound state p:

$$U = \sum_m \langle p|V|p\rangle\ , \tag{23b}$$

where m is the projection quantum number of the state p. The general notation U will be useful in the next section. Definitions (23) are the ones that work best in the DWBA for inelastic scattering[13] and ionization.[14]

IV. NUMERICAL CALCULATION OF THE POLARIZATION POTENTIAL

The partial-wave components of the polarization potential are added to those of the first-order potential to give the partial-wave expansion of the coupled integral equations (19):

$$T_{\bar{l}l\bar{L}L}^{(JS)}(k,k_0) = V_{\bar{l}l\bar{L}L}^{(JS)}(k,k_0) + \sum_{l'L'}\int dq q^2 V_{\bar{l}l'\bar{L}L'}(k,q) \times \frac{1}{E^{(+)}-\varepsilon_{l'}-\frac{1}{2}q^2}T_{l'lL'L}^{(JS)}(q,k_0)\ . \tag{24}$$

For economy of notation we have represented each target state (nonuniquely) by its orbital angular momentum l. The corresponding continuum partial-wave angular momentum is L. The total angular momentum is J. Full notation is given in Ref. 1 together with the method of performing the integration over q.

For the computation we use the coordinate-space representation of the wave functions and potentials. The coordinate-space representation of the quantities in large parentheses in (22) is the Green's function for the potential U projected onto the continuum:

$$G^{(c)}(E-\varepsilon,\mathbf{r},\mathbf{r}')=\int d^3k'\langle \mathbf{r}|\chi^{(-)}(\mathbf{k}')\rangle \times\frac{1}{E^{(+)}-\varepsilon-\frac{1}{2}k'^2}\langle\chi^{(-)}(\mathbf{k}')|\mathbf{r}'\rangle \ . \tag{25}$$

The partial-wave expansion of the full Green's function, which includes both bound and continuum states of the potential U, is

$$G(E-\varepsilon;\mathbf{r},\mathbf{r}')=\sum_{jm} g_j(E-\varepsilon;r,r')Y_{jm}(\hat{\mathbf{r}})Y^*_{jm}(\hat{\mathbf{r}}') \ , \tag{26}$$

where

$$g_j(E-\varepsilon;r,r')=-K^{-1}(rr')^{-1}u_j(K,r_<)h_j(K,r_>) \ , \tag{27}$$

$$\tfrac{1}{2}K^2=E-\varepsilon \ , \tag{28}$$

u_j is the physical partial wave and h_j is asymptotically a spherical outgoing wave, both calculated for the potential U. Their external forms are

$$u_j(K,r)=F_j(K,r)+C_j[G_j(K,r)+iF_j(K,r)] \ , \tag{29}$$

$$h_j(K,r)=G_j(K,r)+iF_j(K,r) \ , \tag{30}$$

where F_j and G_j are the regular and irregular Coulomb functions for the appropriate charge and C_j is a complex matching constant related to the phase shift.

We find an alternative form for $g_j(r,r')$ from the partial-wave expansion of the spectral representation (25) of the full Green's function:

$$g_j(E-\varepsilon;r,r')=\frac{2}{\pi}(rr')^{-1}\int dk' u_j(k',r) \times\frac{1}{E^{(+)}-\varepsilon-\frac{1}{2}k'^2}u_j(k',r') + \sum_n (rr')^{-1}u_{jn}(r)\frac{1}{E^{(+)}-\varepsilon-\varepsilon_{jn}}u_{jn}(r') \ , \tag{31}$$

where $u_j(k,r)$ is the partial wave of $\chi^{(-)}(\mathbf{k},\mathbf{r})$ and $u_{jn}(r)$ is the radial wave function of the bound state jn of the potential U.

To obtain the continuum projection of the partial-wave Green's function we subtract the bound-state terms of (31) from (27):

$$g_j^{(c)}(E-\varepsilon;r,r')=-K^{-1}(rr')^{-1}u_j(K,r_<)h_j(K,r_>) - \sum_n (rr')^{-1}u_{jn}(r) \times\frac{1}{E^{(+)}-\varepsilon-\varepsilon_{jn}}u_{jn}(r') \ . \tag{32}$$

For case 1 of (23), U is the Coulomb potential of the nucleus. There are an infinite number of bound states n to be subtracted in (32) but the sum over n is rapidly convergent. For case 2 the average potentials for hydrogen do not support bound states.

The polarization potential consists of a direct term DD and three exchange terms ED, DE, and EE, where the first (last) D or E refers to the direct (exchange) nature of the first (last) excitation matrix element in (20). The partial-wave polarization potential corresponding to (22) is the sum of four terms with different exchange characters:

$$\bar{V}^{(JS)}_{l\bar{l}L\bar{L}}=\bar{V}^{(J,DD)}_{l\bar{l}L\bar{L}}+\bar{V}^{(J,EE)}_{l\bar{l}L\bar{L}}+(-1)^S(\bar{V}^{(J,DE)}_{l\bar{l}L\bar{L}}+\bar{V}^{(J,ED)}_{l\bar{l}L\bar{L}}) \ . \tag{33}$$

We illustrate the full partial-wave expansion only for the DD case (the others are obtained by the corresponding space exchanges):

$$\begin{aligned}\bar{V}^{(J,DD)}_{l\bar{l}L\bar{L}}(q',q)=&\left[\frac{2}{\pi}\right]^2 i^{L-\bar{L}}(-1)^{\bar{l}+l}(q'q)^{-1} \\ &\times\sum_{jL'\bar{\lambda}\lambda}\int dr\int dr'\hat{j}\hat{L}'\hat{L}\hat{l}\begin{bmatrix}L&\lambda&j\\0&0&0\end{bmatrix}\begin{bmatrix}L'&\lambda&l\\0&0&0\end{bmatrix}\begin{Bmatrix}j&J&L'\\l&\lambda&L\end{Bmatrix} \\ &\times\hat{j}\hat{L}'\hat{\bar{L}}\hat{\bar{l}}\begin{bmatrix}\bar{L}&\bar{\lambda}&j\\0&0&0\end{bmatrix}\begin{bmatrix}L'&\bar{\lambda}&\bar{l}\\0&0&0\end{bmatrix}\begin{Bmatrix}j&J&L'\\\bar{l}&\bar{\lambda}&\bar{L}\end{Bmatrix} \\ &\times\Bigg[\sum_{p\in Q}\left[\int dr'' U_{\bar{L}}(q'r)u_{\bar{l}}(r'')v_{\bar{\lambda}}(r,r'')u_{pL'}(r'')\right] \\ &\quad\times g_j^{(c)}(E-\varepsilon_p;r,r')\left[\int dr''' u_{pL'}(r''')v_{\lambda}(r''',r')u_l(r''')U_L(qr')\right] \\ &\quad+\int dk\left[\int dr'' U_{\bar{L}}(q'r)u_{\bar{l}}(r'')v_{\bar{\lambda}}(r,r'')u_{L'}(k,r'')\right] \\ &\quad\times g_j^{(c)}(E-\tfrac{1}{2}k^2;r,r')\left[\int dr''' u_{L'}(k,r''')v_{\lambda}(r''',r')u_l(r''')U_L(qr')\right]\Bigg] \ .\end{aligned} \tag{34}$$

TABLE I. Total ionization (σ_I), excitation (σ_{ex}), and reaction (σ_R) cross sections (πa_0^2) for electron-hydrogen scattering calculated in the 1-channel weak-coupling approximation (CCO) from the DW optical potential and compared with semiempirical data (Ref. 18) (expt) whose errors are about 10%. CCO1 and CCO3 are weak-coupling calculations with 1 and 3 channels in P space, respectively.

	σ_I		σ_{ex}			σ_R	
E (eV)	CCO	Expt.	CCO1	CCO3	Expt.	CCO	Expt.
30	1.16	0.61	1.71	1.63	1.37	2.79	1.98
50	1.08	0.77	1.40	1.35	1.32	2.44	2.09
100	0.77	0.715	0.98	0.97	1.04	1.74	1.76
200	0.47	0.48	0.63	0.63	0.70	1.10	1.20
400	0.25	0.29	0.37	0.37	0.41	0.62	0.697

For DE we interchange l and L in the angular-momentum coefficients and r''' and r' in the corresponding radial wave functions. For ED we perform a similar interchange for $\bar{l}$ and $\bar{L}$ and for EE we make both exchanges. Here the symbols in large parentheses and curly brackets are Wigner $3j$ and $6j$ symbols, respectively, the symbol u represents a radial wave function in obvious notation, and $\hat{L}$ means $(2L+1)^{1/2}$. The λ multipole of the Coulomb potential is $v_\lambda(r,r')$. The radial bound-state functions $u_l(r)$ are defined in terms of the target eigenfunctions $\langle \mathbf{r}|p \rangle$ by

$$\langle \mathbf{r}|p \rangle = r^{-1}u_l(r)Y_{lm}(\hat{\mathbf{r}}) \tag{35}$$

and $u_l(r)$ is positive for small r.

Convergence in the discrete Q-space sum and in the Green's function (32) is achieved by including bound states up to $n=6, L'=3$. The continuum states need partial waves up to $L'=15$.

TABLE II. The total electron-hydrogen ionization asymmetry A_I calculated by CCO in the weak-coupling approximation compared with the experimental data of Fletcher *et al.* (Ref. 19). The full width at half maximum of the incident energy distribution is also given. The error in the last significant figures of A_I is given in parentheses. The calculation is done at the central energy for each case.

E (eV)	FWHM (eV)	A_I (expt.)[a]	A_I (CCO)
14.1	2.3	0.446(34)	0.431
15.0	3.2	0.529(27)	0.427
17.0	3.2	0.430(26)	0.415
19.0	3.2	0.449(24)	0.402
22.2	2.5	0.436(5)	0.382
27.0	2.7	0.369(5)	0.351
30.3	2.5	0.324(9)	0.334
34.0	3.2	0.307(18)	0.313
42.0	3.2	0.320(11)	0.278
57.0	3.2	0.233(13)	0.229
77.0	3.2	0.184(31)	0.188
107.0	3.2	0.143(11)	0.149
147.0	3.2	0.118(12)	0.118
197.0	3.2	0.071(14)	0.094

[a]Reference 19.

V. WEAK COUPLING: IONIZATION AND EXCITATION

Before testing the whole CCO calculation it will be interesting to see how well the DW polarization potential obeys some of the necessary constraints given by the weak-coupling approximation.[17] In this approximation the total reaction cross section from a 1-channel calculation with the polarization potential for part of Q space is the total cross section for the excitation of that part of Q space. The weak-coupling approximation in the case of the DW polarization potential may be understood as the DWBA with the entrance-channel distorted wave calculated in a spin-dependent, complex, nonlocal optical potential.

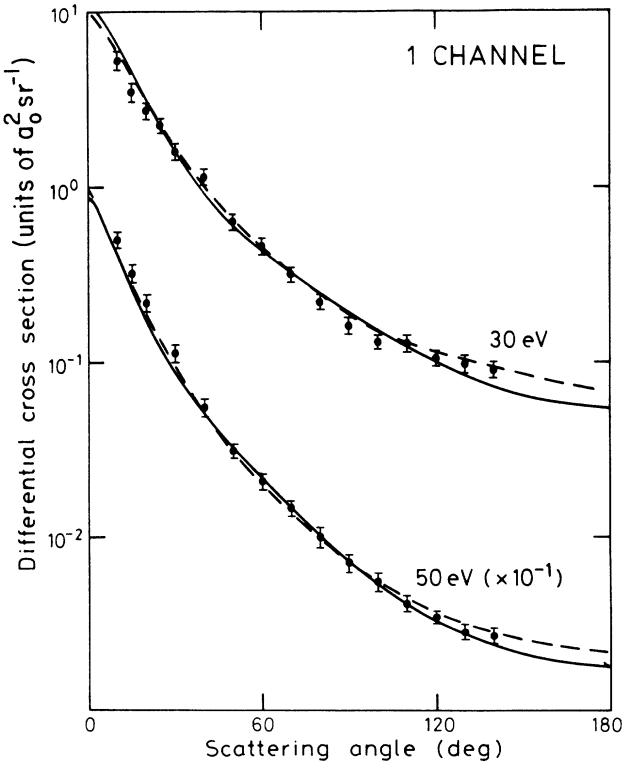

FIG. 1. Differential cross sections for elastic e-H scattering. Solid circles, Williams (Ref. 20); solid curves, 1-channel CCO; dashed curves, IERM (Ref. 6).

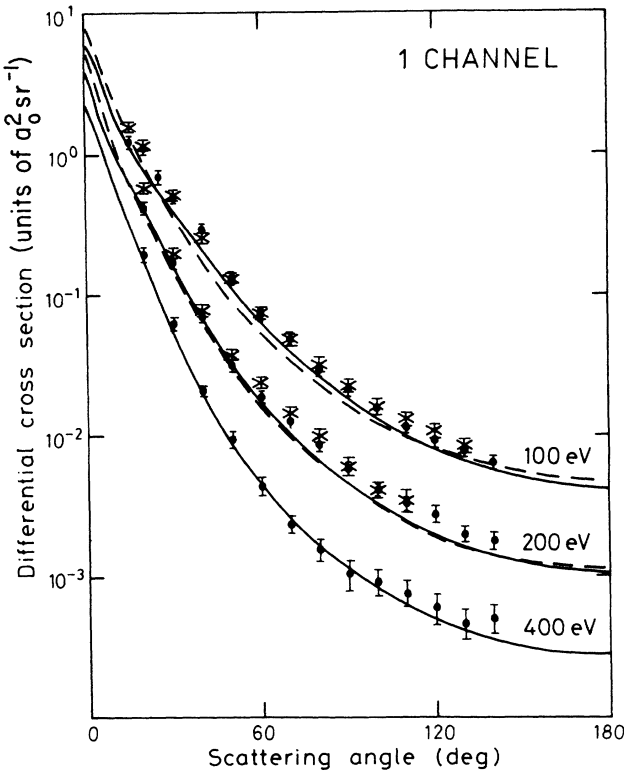

FIG. 2. Differential cross sections for elastic *e-H* scattering. Solid circles, Williams (Ref. 20); crosses, van Wingerden *et al.* (Ref. 21); solid curves, 1-channel CCO; dashed curves, UEBS (Ref. 8).

The relevant quantities for which experimental data exist are the total ionization cross section, the total ionization asymmetry, and the total excitation cross section. Total cross sections for particular discrete excitations also exist but it will be more interesting to compare them with the results of a corresponding CCO calculation (see Sec. VII).

Table I compares the total reaction (σ_R), ionization (σ_I), and excitation (σ_{ex}) cross sections with the corresponding quantities from the semiempirical compilation of de Heer, McDowell, and Wagenaar.[18] The weak-coupling approximation fails to the extent that σ_I and σ_{ex} do not sum to σ_R. The discrepancy is noticeable at the lower energies, but not large enough to make the conclusions drawn from the approximation meaningless. For σ_{ex} the column CCO1 is calculated with the polarization potential for excitation in a 1-channel CCO calculation. For CCO3, σ_{ex} is calculated using the 3-channel CCO method, again with only the excitation part of the polarization potential. At 30 eV both σ_I and σ_{ex} are seriously overestimated by the DW optical potential. One would expect this excessive loss of flux from the entrance channel to manifest itself in the differential cross section for elastic scattering. At 50 eV there is still a 14% overestimate. Since the polarization potential is of second order one might hope that this overestimate would not have a disastrous effect on scattering in *P* space. Above 100 eV we have underestimates.

Table II shows the total ionization asymmetry A_I compared with the experimental data of Fletcher *et al.*[19] This tests the relative contributions of direct and exchange ionization to the continuum polarization poten-

TABLE IV. Cross sections (in atomic units) for 100-eV elastic *e*-H scattering calculated by the 1-channel and 3-channel CCO methods.

θ (deg)	1 channel	3 channel
0	6.50	6.53
10	1.89	1.92
20	0.800	0.783
30	0.398	0.382
40	0.204	0.197
50	0.110	0.107
60	0.0636	0.0624
70	0.0392	0.0387
80	0.0257	0.0255
90	0.0178	0.0178
100	0.0130	0.0130
120	0.007 85	0.007 94
140	0.005 62	0.005 71
160	0.004 59	0.004 72
180	0.004 31	0.004 44
$\sigma_E(\pi a_0^2)$	0.451	0.446
$\sigma_R(\pi a_0^2)$	1.74	1.71

TABLE III. Integrated elastic (σ_E) and total reaction (σ_R) cross sections (πa_0^2) for electron-hydrogen scattering. Errors in the semiempirical estimates (Ref. 18) (expt.) are of the order 10%. The CCO values are calculated with one channel in *P* space.

	σ_E				σ_R			
E (eV)	Expt.[a]	CCO	UEBS[b]	PS[c]	Expt.[a]	CCO	UEBS[b]	PS[c]
30	2.01	2.08		1.96	1.98	2.79		1.75
50	1.00	1.10			2.09	2.44		
100	0.60	0.451	0.46	0.47	1.76	1.74	1.78	1.69
200	0.22	0.195	0.196		1.20	1.10	1.15	
400	0.065	0.089		0.0872	0.70	0.62		0.64

[a]Reference 18.
[b]Reference 8.
[c]Reference 22.

TABLE V. Partial cross sections (πa_0^2) for the $1s$, $2s$, and $2p$ ($S=0$ and 1) channels, $J=0,1$, and 2 at 54.42 eV. The present calculation (CCO) is compared with that of Scholz *et al.* (Ref. 23) (IERM). Numbers in square brackets denote powers of 10.

J	State	CCO ($S=0$)	IERM ($S=0$)	CCO ($S=1$)	IERM ($S=1$)
0	$1s$	6.16[−2]	6.68[−2]	4.12[−1]	4.03[−1]
	$2s$	3.1[−3]	2.79[−3]	3.3[−3]	2.19[−3]
	$2p$	4.1[−3]	3.07[−3]	5.1[−3]	5.23[−3]
1	$1s$	2.85[−2]	2.52[−2]	2.80[−1]	2.71[−2]
	$2s$	6.5[−3]	7.75[−3]	9.8[−3]	1.00[−2]
	$2p$	4.3[−3]	4.09[−3]	5.4[−3]	5.04[−3]
2	$1s$	1.69[−2]	1.47[−2]	8.75[−2]	8.30[−2]
	$2s$	3.9[−3]	3.69[−3]	1.08[−2]	1.23[−2]
	$2p$	1.71[−2]	1.21[−2]	1.27[−2]	1.40[−2]

tial. Here the DW polarization potential is spectacularly successful at all energies, even near threshold.

VI. ENTRANCE CHANNEL

The simplest CCO calculation of entrance-channel phenomena, namely the elastic differential and integrated cross sections and the total reaction cross section, is done with P space consisting of just the entrance channel. All other channels are included in the DW optical potential.

Figure 1 shows the elastic differential cross sections for 30 and 50 eV compared with the experimental data of Williams.[20] The result of the IERM method[6] is also shown. The CCO method is perhaps surprisingly good, in view of the overestimate of the total reaction cross section which must affect the elastic cross section.

Elastic differential cross sections at 100, 200, and 400 eV are shown in Fig. 2, compared with the experimental data of Williams[20] and van Wingerden *et al.*[21] At these energies the method describes elastic scattering very well.

TABLE VI. Differential cross sections (a_0^2/sr), $\sigma_E(\pi a_0^2)$ for elastic e-H scattering. The CCO uses the $1s,2s,2p$ P space. Errors in the final significant figures are given in parentheses. Numbers in square brackets indicate powers of 10.

	54.4 eV		100 eV			200 eV		
θ (deg)	Expt.[a]	CCO	Expt.[c]	Expt.[d]	CCO	Expt.[c]	Expt.[d]	CCO
0		8.99[0]			6.53[0]			4.42[0]
10	4.98(51)[0]	3.79[0]			1.92[0]			1.01[0]
15	3.12(37)[0]	2.38[0]		1.59(11)[0]	1.18[0]	1.22(12)[0]		6.27[−1]
20	2.07(23)[0]	1.57[0]	1.10(10)[0]	1.17(8)[0]	7.83[−1]	4.19(40)[−1]	5.77(48)[−1]	3.91[−1]
25	1.36(21)[0]	1.09[0]	6.92(71)[−1]		5.44[−1]			2.44[−1]
30	1.06(12)[0]	7.91[−1]	5.09(49)[−1]	5.25(35)[−1]	3.82[−1]	1.72(17)[−1]	2.00(15)[−1]	1.55[−1]
40	5.22(59)[−1]	4.55[−1]	2.88(27)[−1]	2.57(21)[−1]	1.97[−1]	7.06(68)[−2]	7.74(73)[−2]	6.67[−2]
50	2.89(27)[−1]	2.81[−1]	1.32(12)[−1]	1.31(10)[−1]	1.07[−1]	3.14(32)[−2]	3.79(32)[−2]	3.20[−2]
60	1.89(19)[−1]	1.82[−1]	7.22(71)[−2]	7.4(8)[−2]	6.24[−2]	1.87(19)[−2]	2.37(23)[−2]	1.72[−2]
70	1.35(14)[−1]	1.23[−1]	4.91(46)[−2]	4.8(5)[−2]	3.87[−2]	1.25(14)[−2]	1.45(13)[−2]	1.02[−2]
80	9.12(121)[−2]	8.59[−2]	2.95(30)[−2]	3.19(34)[−2]	2.55[−2]	8.59(92)[−3]	1.00(10)[−2]	6.53[−3]
90	6.62(82)[−2]	6.23[−2]	2.09(20)[−2]	2.27(20)[−2]	1.78[−2]	5.84(61)[−3]	6.2(8)[−3]	4.46[−3]
100	5.15(66)[−2]	4.68[−2]	1.55(15)[−2]	1.62(20)[−2]	1.30[−2]	4.12(42)[−3]	4.11(51)[−3]	3.22[−3]
110	3.86(43)[−2]	3.65[−2]	1.15(12)[−2]	1.30(15)[−2]	9.96[−3]	3.23(31)[−3]	3.47(60)[−3]	2.46[−3]
120	3.20(33)[−2]	2.94[−2]	9.2(9)[−3]	1.07(12)[−2]	7.94[−3]	2.72(35)[−3]		1.96[−3]
130	2.63(30)[−2]	2.46[−2]	7.8(7)[−3]	8.4(9)[−3]	6.61[−3]	1.99(25)[−3]		1.64[−3]
140	2.49(26)[−2]	2.13[−2]	6.5(7)[−3]		5.71[−3]	1.78(26)[−3]		1.41[−3]
160		1.76[−2]			4.72[−3]			1.17[−3]
180		1.65[−2]			4.44[−3]			1.18[−3]
σ_E[e]	9.65[−1][b]	9.81[−1]		6.0[−1]	4.46[−1]		2.2[−1]	1.94[−1]
σ_R[e]	2.07[0][b]	2.20[0]		1.76[0]	1.71[0]		1.20[0]	1.09[0]

[a]Cubic spline interpolation in the table of Williams (Ref. 20).
[b]Linear interpolation in the table of de Heer *et al.* (Ref. 18).
[c]Reference 20.
[d]Reference 21.
[e]Reference 18.

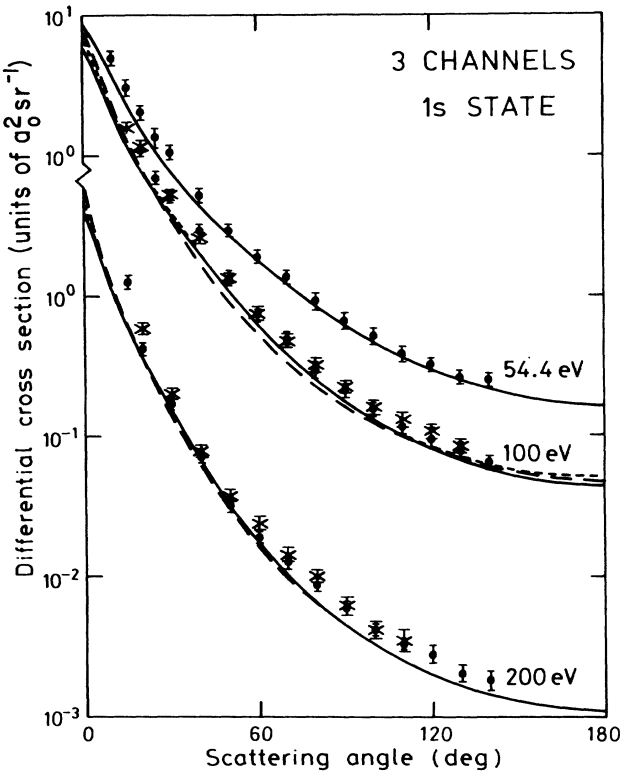

FIG. 3. Differential cross sections for elastic *e-H* scattering. Solid circles, Williams (Ref. 20); crosses, van Wingerden *et al.*, (Ref. 21); solid curves, 3-channel CCO; long-dashed curves, UEBS (Ref. 8); short-dashed curves, PS (Ref. 9).

It is compared with the UEBS.[8]

The integrated elastic σ_E and total reaction σ_R cross sections are given in Table III in comparison with the semiempirical data of de Heer *et al.*[18] The results of two other elastic channel calculations are included. They are UEBS (Ref. 8) and the pseudostate optical potential calculation PS of Callaway and Unnikrishnan.[22] There is little to choose between the calculations of σ_E, but it has proved possible to find a set of pseudostate parameters that outperforms the CCO method for σ_R at 30 eV. PS (Ref. 22) also gives elastic differential cross sections that are better than CCO at 30 eV and very close at higher energies.

It is not considered worthwhile to give tables of numerical differential cross sections for the 1-channel calculation. Full details are given in Sec. VII for the 3-channel calculation.

VII. THREE-CHANNEL *P* SPACE

The CCO calculation has been done at 54.4, 100, and 200 eV for *P* space consisting of the 1*s*, 2*s*, and 2*p* channels. It is interesting first to consider the 1*s* channel where we can test the validity of the discrete polarization potential for the 2*s* and 2*p* channels by comparing results of calculations that include these channels either in *P* space or *Q* space.

Table IV compares 1*s* cross sections at 100 eV calculated by the 1-channel and 3-channel CCO methods. Differences are no more than about 3%. The column CCO3 in Table I gives the total excitation cross sections

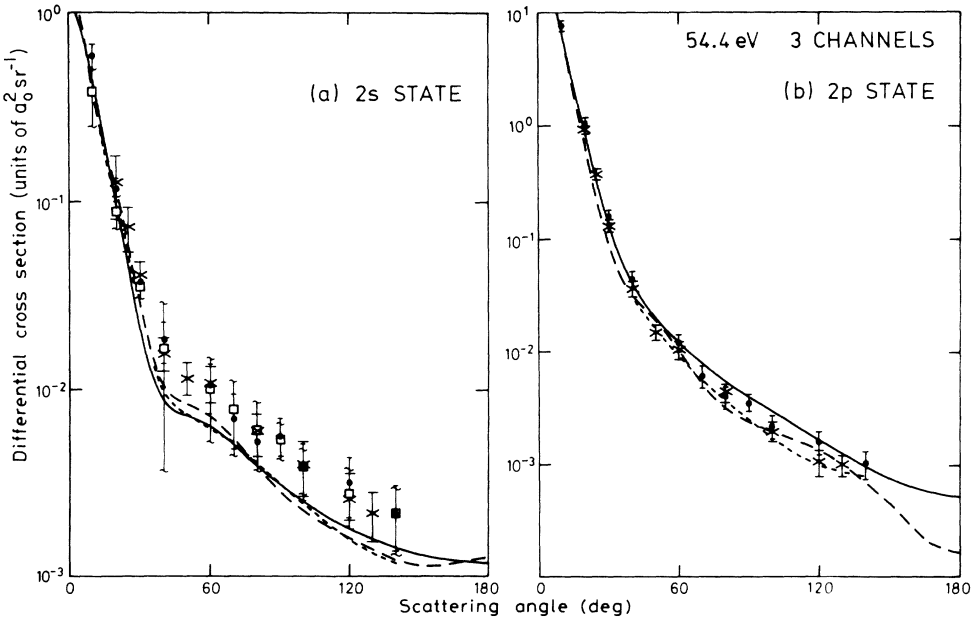

FIG. 4. Differential cross sections for the (a) 2*s* and (b) 2*p* excitation of hydrogen at 54.4 eV. Solid circles, Williams (Ref. 25) (method 2); open squares, Williams (Ref. 25) (method 1); crosses, Frost and Weigold (Ref. 24); solid curves, CCO; long-dashed curves, IERM (Ref. 6); short-dashed curves, PS (Ref. 9).

TABLE VII. Differential cross sections (a_0^2/sr) and integrated cross section $\sigma_{2s}(\pi a_0^2)$ for the $2s$ excitation of hydrogen at 54.4 eV. Errors in the final significant figures are given in parentheses. Numbers in square brackets indicate powers of 10.

θ (deg)	Expt.[a]	Expt.[b]	Expt.[d]	CCO
0				1.32[0]
10	3.80(128)[−1]	5.94(94)[−1]		4.38[−1]
20	9.0(18)[−2]	1.16(17)[−1]	1.28(47)[−1]	1.00[−1]
25			7.4(20)[−2]	4.46[−2]
30	3.5(39)[−2]	3.75(40)[−2]	4.09(69)[−2]	2.07[−2]
40	1.65(128)[−2]	1.84(47)[−2]	1.57(31)[−2]	8.63[−3]
50			1.15(22)[−2]	7.33[−3]
60	1.01(48)[−2]	1.06(31)[−2]	1.09(24)[−2]	6.26[−3]
70	7.9(34)[−3]	7.04(218)[−3]		5.04[−3]
80	6.15(247)[−3]	5.27(163)[−3]	5.9(15)[−3]	3.96[−3]
90	5.43(117)[−3]	5.70(128)[−3]		3.13[−3]
100	3.85(105)[−3]	3.85(129)[−3]	4.0(13)[−3]	2.52[−3]
120	2.82(98)[−3]	3.21(114)[−3]	2.6(10)[−3]	1.80[−3]
130			2.18(68)[−3]	1.58[−3]
140	2.18(87)[−3]	2.24(87)[−3]		1.43[−3]
160				1.25[−3]
180				1.23[−3]
$\sigma_{2s}(\pi a_0^2)$			5.6(4)[−2][c]	6.24[−2]

[a]Williams (Ref. 25) method 1.
[b]Williams (Ref. 25) method 2.
[c]van Wyngaarden and Walters (Ref. 9).
[d]Reference 24.

at different energies calculated in a 3-channel weak-coupling approximation in which the only polarization potential included is the excitation part. The excitation part excludes $2s$ and $2p$, since they are explicitly coupled in P space. Comparison with CCO1 for excitation shows that it is advantageous to include the lower excitations in P space at the lower energies, but the DW polarization potential represents them very well at the higher energies.

It is interesting to compare some details of the 3-channel CCO calculation with the other detailed fully mi-

TABLE VIII. Differential cross sections (a_0^2/sr) and integrated cross section (πa_0^2) for the $2p$ excitation of hydrogen at 54.4 eV. Errors in the final significant figures are given in parentheses. Numbers in square brackets indicate powers of 10.

θ (deg)	Expt.[a]	Expt.[c]	CCO
0			4.01[1]
10	7.54(71)[0]		6.97[0]
20	1.04(11)[0]	9.12(69)[−1]	8.61[−1]
25		3.73(36)[−1]	3.29[−1]
30	1.57(21)[−1]	1.32(16)[−1]	1.39[−1]
40	4.36(69)[−2]	3.64(58)[−2]	4.10[−2]
50		1.50(23)[−2]	2.06[−2]
60	1.19(21)[−2]	1.04(18)[−2]	1.23[−2]
70	6.12(131)[−3]		8.08[−3]
80	4.05(87)[−3]	4.38(80)[−3]	5.65[−3]
90	3.56(56)[−3]		4.09[−3]
100	2.16(46)[−3]	1.97(38)[−3]	3.01[−3]
120	1.59(36)[−3]	1.08(28)[−3]	1.67[−3]
130		1.02(21)[−3]	1.25[−3]
140	1.03(28)[−3]		9.57[−4]
160			6.34[−4]
180			5.38[−4]
$\sigma_{2p}(\pi a_0^2)$	0.89(8)[a]	0.72(3)[b]	0.815

[a]Williams (Ref. 25).
[b]van Wyngaarden and Walters (Ref. 9).
[c]Reference 24.

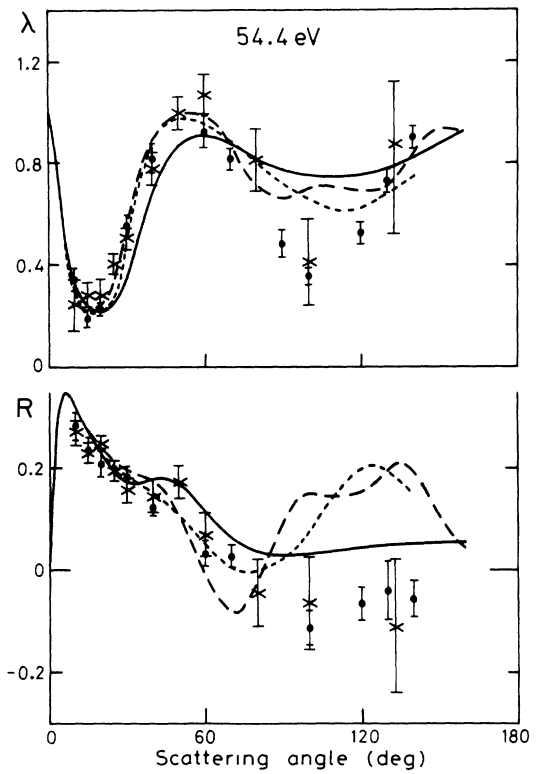

FIG. 5. The angular correlation parameters λ and R for the $2p$ excitation of hydrogen at 54.4 eV. Solid circles, Williams (Ref. 25); crosses, Hood *et al.* (Ref. 27) ($\theta \leq 20°$), Weigold *et al.* (Ref. 28) ($\theta > 20°$). Curves as for Fig. 4.

croscopic calculation that has been done, namely the IERM method,[23] for total angular momenta 0, 1, and 2. In Table V we compare the partial cross sections for the three channels at 54.42 eV. There are no qualitative discrepancies.

A. The 1s channel

Numerical cross sections for the 3-channel CCO calculation are compared with experiment in Table VI. At 54.4 eV the experimental values are obtained by cubic spline interpolation in the table of Williams.[20] Errors are those of the 50-eV experiment. Differential cross sections are compared with experiment in Fig. 3.

In general the CCO differential cross sections are less than the experimental values, particularly at smaller angles where they are well outside the experimental error limits. Comparing CCO with other calculations at 100 eV, the UEBS (Ref. 8) does better at small and large angles, but considerably worse over most of the angular distribution. The 3-channel PS calculation of van Wyngaarden and Walters[9] is very similar to CCO over most of the range but somewhat better at small and large angles. However, the differences between calculations are smaller than the experimental errors. At 200 eV, differences between the same three calculations are almost imperceptible. Overall the agreement between calculations is very significant compared with the discrepancy between calculations and experiment.

B. The 2s channel

The $2s$ and $2p$ differential cross sections have been experimentally separated at 54.4 eV by Frost and Weigold[24] and Williams.[25] The CCO cross sections for $2s$ are compared with experimental data in Fig. 4(a) together with two detailed calculations IERM (Ref. 6) and PS.[9] All calculated cross sections are somewhat lower than the central experimental values. Differences between the three calculations are much smaller than the experimental errors.

Numerical values of CCO differential and integrated cross sections are compared with experiment in Table

TABLE IX. The angular correlation parameters λ and R for the $2p$ excitation of hydrogen at 54.4 eV. Errors in the final significant figures are given in parentheses. Numbers in square brackets indicate powers of 10.

	λ			R		
θ (deg)	Expt.[a]	Expt.[b]	CCO	Expt.[a]	Expt.[b]	CCO
10	3.41(45)[−1]	2.42[−1]	3.38[−1]	2.83(27)[−1]	2.71[−1]	3.22[−1]
15	1.88(32)[−1]	2.80[−1]	2.39[−1]	2.35(25)[−1]	2.30[−1]	2.69[−1]
20	2.25(25)[−1]	2.81[−1]	2.15[−1]	2.08(23)[−1]	2.49[−1]	2.25[−1]
25		4.04(49)[−1]	2.46[−1]		1.94(20)[−1]	1.9[−1]
30	5.53(39)[−1]	5.03(42)[−1]	3.45[−1]	1.81(21)[−1]	1.55(24)[−1]	1.7[−1]
40	8.17(56)[−1]	7.78(62)[−1]	6.69[−1]	1.22(18)[−1]	1.49(34)[−1]	1.79[−1]
50		9.95(64)[−1]	8.61[−1]		1.74(34)[−1]	1.68[−1]
60	9.22(62)[−1]	1.07(8)°	9.05[−1]	8.2(26)[−2]	6.8(41)[−2]	1.16[−1]
70	9.16(39)[−1]		8.75[−1]	2.7(21)[−2]		6.53[−2]
80		8.1(12)[−1]	8.21[−1]		−4.5(64)[−2]	3.76[−2]
90	4.83(52)[−1]		7.74[−1]	−5.1(29)[−2]		3.07[−2]
100	3.54(33)[−1]	4.1(17)[−1]	7.50[−1]	−1.13(33)[−1]	−6.5(90)[−2]	3.28[−2]
120	5.25(42)[−1]		7.53[−1]	−6.51(31)[−2]		4.40[−2]
130	7.27(45)[−1]		7.76[−1]	−4.0(57)[−2]		4.78[−2]
133		8.7(25)[−1]	7.86[−1]		−1.1(13)[−1]	4.89[−2]
140	9.01(43)[−1]		8.13[−1]	−5.6(35)[−2]		5.31[−2]

[a]Williams (Ref. 25).

[b]$\theta \leq 20°$: Hood *et al.* (Ref. 27); $\theta > 20°$: Weigold *et al.*[28] (Ref. 28).

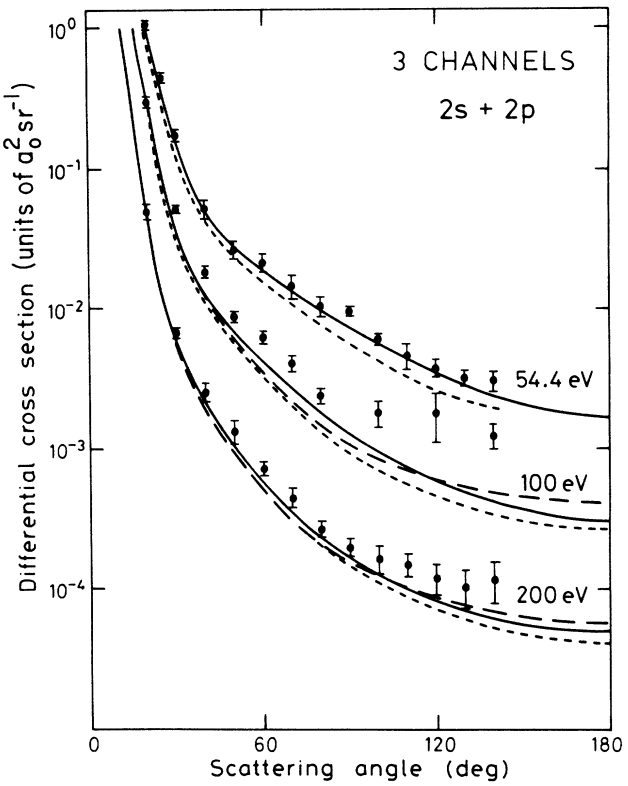

FIG. 6. Summed differential cross sections for the $n=2$ excitations of hydrogen. Solid circles, Williams and Willis (Ref. 29); solid curves, CCO; long-dashed curves, UEBS (Ref. 8); short-dashed curves, PS (Ref. 9).

VII. There is an experimental anomaly. The CCO differential cross section consistently underestimates the experimental values, yet the integrated cross section is significantly greater than the value obtained by van Wyngaarden and Walters[9] by allowing for cascade corrections to the independent experiment of Kauppila *et al.*[26]

C. The 2p channel

Differential cross sections for the $2p$ channel at 54.4 eV are given in Table VIII and Fig. 4(b) for the same calculations and experiments as the $2s$ cross sections. The difference between calculations is of the order of the experimental error. CCO agrees better with the large forward cross sections than the other calculations. The CCO value for σ_{2p} lies between the value quoted by van Wyngaarden and Walters[9] and the independent measurement of Williams.[25]

Other important observables that have been measured at 54.4 eV are the angular correlation parameters λ and R. The experimental values are compared with the calculations CCO, IERM,[6] and PS (Ref. 9) in Fig. 5. Numerical values are given in Table IX. CCO has more difficulty than the other calculations in describing the width of the first minimum and the depth of the second minimum for λ, but it gives a markedly improved description of R.

D. Summed n=2 channels

The sum of the differential cross sections for the $n=2$ channels has been measured by Williams and Willis (Ref. 29). Figure 6 compares the CCO result with these data, together with the results of UEBS (Ref. 8) and PS.[9] Table X gives the numerical values for 54, 100, and 200 eV.

The CCO differential cross sections are very close to the experimental values at 54 eV, in general slightly below the central experimental values. The CCO integrated cross sections at 54 eV are significantly higher than the independent semiempirical values of van Wyngaarden and Walters.[9] This experimental anomaly is intensified at 100 eV, where the CCO values are well below the differential cross sections of the experiment, although the integrated cross sections are close to (but slightly larger than) the semiempirical estimates. At 200

TABLE X. Differential (a_0^2/sr) and integrated (πa_0^2) cross sections for the summed $n=2$ excitations of hydrogen at 54, 100, and 200 eV. Errors in the final significant figures are given in parentheses; numbers in square brackets indicate powers of 10.

	54 eV		100 eV		200 eV	
θ (deg)	Expt. (Ref. 29)	CCO	Expt.	CCO	Expt.	CCO
20	1.04(7)[0]	9.68[−1]	2.97(25)[−1]	3.17[−1]	4.97(57)[−2]	5.12[−2]
25	4.47(34)[−1]	3.76[−1]		9.54[−2]		1.34[−2]
30	1.72(20)[−1]	1.60[−1]	5.19(23)[−2]	3.61[−2]	6.72(61)[−3]	5.59[−3]
40	5.21(81)[−1]	4.92[−2]	1.82(16)[−2]	1.24[−2]	2.54(38)[−3]	2.18[−3]
50	2.65(39)[−2]	2.77[−2]	8.73(62)[−3]	6.85[−3]	1.32(24)[−3]	1.03[−3]
60	2.13(33)[−2]	1.88[−2]	6.19(57)[−3]	4.15[−3]	7.27(72)[−4]	5.83[−4]
70	1.44(27)[−2]	1.32[−2]	4.07(41)[−3]	2.68[−3]	4.48(66)[−4]	3.45[−4]
80	1.03(16)[−2]	9.56[−3]	2.38(29)[−3]	1.80[−3]	2.71(33)[−4]	2.35[−4]
90	9.47(59)[−3]	7.22[−3]		1.27[−3]	1.99(29)[−4]	1.69[−4]
100	5.98(61)[−3]	5.53[−3]	1.82(37)[−3]	9.44[−4]	1.66(36)[−4]	1.25[−4]
110	4.57(87)[−3]	4.36[−3]		7.23[−4]	1.51(28)[−4]	9.91[−4]
120	3.72(58)[−3]	3.51[−3]	1.79(68)[−3]	5.84[−4]	1.20(29)[−4]	8.07[−5]
130	3.20(38)[−3]	2.82[−3]		4.86[−4]	1.04(31)[−4]	6.91[−5]
140	3.04(47)[−3]	2.38[−3]	1.25(25)[−3]	4.18[−4]	1.17(39)[−4]	5.93[−5]
σ_{2s} [a]	5.6(5)[−2]	6.23[−2]	3.9(4)[−2]	4.44[−2]	2.5(3)[−2]	2.63[−2]
σ_{2p} [a]	7.2(3)[−1]	8.19[−1]	6.2(3)[−1]	6.62[−1]	4.5(2)[−1]	4.52[−1]

[a]Reference 9.

TABLE XI. The ratio of $n=1$ to $n=2$ differential cross sections. Errors in the final significant figures are given in parentheses.

E (eV)	Result	Scattering angle (deg) 30	45	60
100	Expt[a]	11.4(7)	14.5(8)	14.8(8)
	CCO	10.6	16.1	15.0
	PS[b]	13.0	19.3	18.2
	UEBS[c]	10.0	14.6	15.1
200	Expt	25.4(14)	28.8(15)	35.8(25)
	CCO	27.8	30.6	29.7
	PS	29.4	34.4	31.0
	UEBS	30.0	45.0	34.0

[a]Reference 30.
[a]Reference 9.
[a]Reference 8.

eV, CCO agrees quite well with all the experiments, although it is still below the differential cross section data in general. CCO is significantly better than the other two calculations at all energies.

E. Ratios of $n=1$ to $n=2$ cross sections

In view of the anomalies between independent experiments and of the fact that differences between completely different calculations were, before CCO, generally smaller than the theoretical-experimental differences, an independent and accurate experiment on the ratio of the $n=1$ to $n=2$ differential cross sections at 100 and 200 eV was reported by Lower, McCarthy, and Weigold.[30] Table XI compares these experimental data with CCO, PS,[9] and UEBS.[8]

Although CCO is the best of the three calculations, UEBS is very close. We note that the UEBS differential cross sections are below the CCO values for both $n=1$ and $n=2$ and further away from experiment.

VIII. CONCLUSIONS

The CCO method is a fully microscopic calculation of electron-atom scattering in the sense that every aspect of the collision is calculated *ab initio*. Target states are treated in a good approximation (exactly in the case of hydrogen). The scattering set P of target states is treated by solving the relevant coupled integral equations. Excitation of the remaining target states (Q space) is treated by making the distorted-wave Born approximation to the corresponding complete scattering wave functions in the optical potential. All aspects of the collision are interdependent in the calculation. States are fully antisymmetrized. Numerical truncations are carried out to complete convergence, aiming at an overall accuracy of 1%.

The internal consistency of the calculation for discrete target states is checked for hydrogen by including the $n=2$ states either in P space or the optical potential. Elastic differential cross sections and total reaction cross sections agree extremely well at energies of 100 eV or more. At lower energies it is advantageous to include lower target states in P space rather than Q space.

There is no internal check for the target continuum. The DWBA treatment is tested by calculating the total ionization cross section in the weak-coupling approximation. Agreement with experiment is achieved at 100 eV or more. The calculation gives overestimates at lower energies. The DWBA for ionization is checked independently of the CCO calculation by comparing it with experimental differential cross sections.[14] It gives a good account of the larger cross sections that contribute most to the kinematic integration in the optical potential.

The treatment of antisymmetry is very closely confirmed by comparing total ionization asymmetries, calculated in the weak-coupling approximation, with experiment.

Comparison with completely different theoretical methods is achieved only by looking at the results for various scattering observables. The other microscopic method (in principle) is the intermediate-energy R-matrix (IERM) method, which has so far been calculated[6] only for hydrogen up to a total angular momentum $J=4$. This method involves enormous computational labor. A complete 3-channel CCO calculation for hydrogen (81 values of the total angular momentum J) takes 50 h on the SUN4/280. A 1-channel calculation takes 4 h. The implementation of the IERM method by Scholz *et al.*[6] involves the standard R-matrix calculation with pseudostates at intermediate angular momenta J and the second Born approximation for higher J values. Comparison has also been made here with the unitarized eikonal-Born series (UEBS),[8] which agrees closely with some experimental data at higher energies.

A method that is structurally similar to CCO is the pseudostate (PS) method, which represents Q space by a multiparameter ansatz. The need to include target continuum partial waves up to at least $L'=15$ shows that pseudostates up to $L'=2$ or 3 cannot be regarded in any sense as a discrete representation of a partial-wave-expanded continuum. Nevertheless, Callaway and Unnikrishnan[22] and van Wyngaarden and Walters[9] have shown that it is possible to choose pseudostates that reproduce some experimental data well.

We summarize the results of the CCO method for the

scattering observables in the $1s$, $2s,2p$ P space by observing that it gives a very good overall account of these quantities at energies of 54.4 eV or more. In general, differential cross sections are slightly lower than the experimental values. This has characterized the comparison of previous calculations with experiment, but the effect is less marked for CCO. A very pleasing feature is the overall qualitatively correct description of the detailed experiments at 54.4 eV for the $2p$ channel. The angular distributions of all three quantities $d\sigma_{2p}/d\Omega$, λ, and R are qualitatively described, although details remain to be explained. Previous calculations have not given such a good account of all three quantities, although individual ones, particularly λ, have been better.

The only feature of the CCO method that can be improved is the description of the three-body wave functions for excitations in Q space, although comparison of the effect of including the $n=2$ channels in either P space or Q space confirms that the DWBA works well for discrete states in the context. For continuum target states, however, CCO, in common with other scattering methods, does not include the correct three-body boundary condition for the ionization space. Nevertheless, total ionization cross sections at 100 eV or more are well described and total ionization asymmetries are excellent at all energies.

ACKNOWLEDGMENTS

We would like to acknowledge support by the Australian Research Council, the National Science Foundation, and a Northwest Area Foundation grant of the Research Corporation. We are grateful to Dr. T. Scholz and Professor P. G. Burke for prepublication information.

[1]I. E. McCarthy and A. T. Stelbovics, Phys. Rev. A **28** 2693 (1983).
[2]I. Bray, I. E. McCarthy, J. Mitroy, and K. Ratnavelu, Phys. Rev. A **39**, 4998 (1989).
[3]I. E. McCarthy and A. T. Stelbovics, Phys. Rev. A **22**, 502 (1980).
[4]K. Ratnavelu and I. E. McCarthy, J. Phys. B (to be published).
[5]I. Bray, D. H. Madison, and I. E. McCarthy, Phys. Rev. A **40**, 2820 (1989).
[6]T. T. Scholz, H. R. J. Walters, P. G. Burke, and M. P. Scott, J. Phys. B (to be published).
[7]M. P. Scott, T. T. Scholz, H. R. J. Walters, and P. G. Burke, J. Phys. B **22**, 3055 (1989).
[8]F. W. Byron, Jr., C. J. Joachain, and R. M. Potvliege, J. Phys. B **18**, 1637 (1985).
[9]W. L. van Wyngaarden and H. R. J. Walters, J. Phys. B **19**, 929 (1986).
[10]J. Callaway, Phys. Rep. **45**, 89 (1978); D. H. Madison and J. Callaway, J. Phys. B **20**, 4197 (1987).
[11]D. H. Madison, J. A. Hughes, and D. S. McGinness, J. Phys. B **18**, 2737 (1985).
[12]D. H. Madison (unpublished).
[13]D. H. Madison and K. H. Winters, J. Phys. B **16**, 4437 (1983); D. H. Madison, K. H. Winters, and S. L. Downing, *ibid.* **22**, 1651 (1989); K. Bartschat and D. H. Madison, *ibid.* **21**, 153 (1988); **20**, 5839 (1987); **20**, 1609 (1987).
[14]I. E. McCarthy and X. Zhang, Aust. J. Phys. (to be published).
[15]M. Brauner, J. S. Briggs, and H. Klar, J. Phys. B **22**, 2265 (1989).
[16]A. T. Stelbovics and B. H. Bransden, J. Phys. B **22**, L451 (1989).
[17]I. E. McCarthy and A. T. Stelbovics, Phys. Rev. A **22**, 502 (1980).
[18]F. J. de Heer, M. R. C. McDowell, and R. W. Wagenaar, J. Phys. B **10**, 1945 (1977).
[19]G. D. Fletcher, M. J. Alguard, T. J. Gay, V. W. Hughes, P. F. Wainwright, M. S. Lubell, and W. Raith, Phys. Rev. A **31**, 2854 (1985).
[20]J. F. Williams, J. Phys. B **8**, 2191 (1975).
[21]B. van Wingerden, E. Weigold, F. J. de Heer, and K. J. Nygaard, J. Phys. B **10**, 1345 (1977).
[22]J. Callaway and K. Unnikrishnan, Phys. Rev. A **40**, 1660 (1989).
[23]T. Scholz, P. Scott, and P. G. Burke, J. Phys. B **21**, L139 (1988).
[24]L. Frost and E. Weigold, Phys. Rev. Lett. **45**, 247 (1980).
[25]J. F. Williams, J. Phys. B **14**, 1197 (1981).
[26]W. E. Kauppila, W. R. Ott, and W. L. Fite, Phys. Rev. A **1**, 1099 (1970).
[27]S. T. Hood, E. Weigold, and A. J. Dixon, J. Phys. B **12**, 631 (1979).
[28]E. Weigold, L. Frost, and K. J. Nygaard, Phys. Rev. A **21**, 1950 (1980).
[29]J. F. Williams and B. A. Willis, J. Phys. B **8**, 1641 (1975).
[30]J. Lower, I. E. McCarthy, and E. Weigold, J. Phys. B **20**, 4571 (1987).